electron-diffraction data, and argues strongly that dynamical effects play at most a minor part in influencing the diffraction amplitudes. This is even more significant when we consider that this crystal contains no light elements and, as judged from the transparency of the crystals, were not thinner than normal for specimens used for HREM and SAED investigations. The samples were prepared by standard techniques; they were crushed in an agate mortar, and the thinnest crystals were selected for imaging and diffraction analysis. Electron-diffraction patterns from other crystals were all similar to the series used here. We did not determine the thickness of the crystals, but estimate them to be between 50 and 150 Å thick, which are quite normal values. (For more detailed crystallographic data, see Supplementary Information.)

The atoms shifted on average by 0.2 Å in the refinement. The standard deviations of refined atomic positions calculated by SHELXL-93 ranged from 0.015 to 0.021 A. The average accuracy in atomic positions obtained here by electron crystallography (0.02 Å) is close to what may be expected from refinement against X-ray diffraction data. The temperature factors were about twice as high for the Se atoms as for the Ti atoms.

The structure of $Ti_{11}Se_4$ has many features in common with the other structures in the Ti–Se system. In particular, $Ti_{11}Se_4$ and Ti_8Se_3 are closely related, as seen from Fig. 4, which shows the underlying common construction set. Note that every second layer consists of alternating strings of two and four condensed octahedra chains in both structures. The distortions of the octahedra in the equivalent motifs are remarkably similar. This is a very strong argument in favour of the reliability of our refinement.

Electron crystallography opens a window into the vast world of microcrystalline compounds, natural as well as synthetic, including minerals, alloys and other new materials. With slight modifications, electron crystallography might be further extended to provide atomic positions in ordered structures which are not crystalline in the traditional sense. These include defects, interfaces and quasi-crystals. □

Received 14 March; accepted 30 May 1996.

1. DeRosier, D. J. & Klug, A. *Nature* **217,** 130–134 (1968).
2. Cowley, J. M. *Diffraction Physics* 2nd edn (North-Holland, Amsterdam, 1984).
3. Atkins, P. W. *Physical Chemistry* 5th edn (Oxford Univ. Press, 1994).
4. Gjønnes, J. & Steeds, J. W. in *International Tables for Crystallography* Vol. C, (ed. Wilson, A. J. C.) 363–365 (Kluwer Academic, Dordrecht, 1992).
5. Hovmöller, S., Sjögren, A., Farrants, G., Sundberg, M. & Marinder, B.-O. *Nature* **311,** 238–241 (1984).
6. Downing, K. H., Hu, M., Wenk, H.-R. & O'Keefe, M. A. *Nature* **348,** 525–528 (1990).
7. Hovmöller, S. *Trans. Am. Cryst. Ass.* **28,** 95–103 (1992).
8. Simon, A. *Angew. Chem. int. Edn. engl.* **20,** 1–22 (1981).
9. Owens, J. P. & Franzen, H. F. *Acta Crystallogr.* **B30,** 427–430 (1974).
10. Weirich, T. E., Simon, A. & Pöttgen, R. *Z. Anorg. Allg. Chem.* **622,** 630–634 (1996).
11. Weirich, T. E., Pöttgen, R. & Simon, A. *Z. Kristallogr.* (in the press).
12. Weirich, T. E., Pöttgen, R. & Simon, A. *Z. Kristallogr.* (in the press).
13. Goldstein, J. J. in *Introduction to Analytical Electron Microscopy* (eds Hren, J. J., Goldstein, J. I. & Joy, D. C.) 83–120 (Plenum, New York, 1979).
14. Sheldrick, G. M. *Acta Crystallogr.* **A46,** 467–473 (1990); *SHELXL-93, Program for Crystal Structure Refinement* (Göttingen, 1993).
15. Doyle, P. A. & Turner, P. S. *Acta crystallogr.* **A24,** 390–397 (1968).
16. Hovmöller, S. *Ultramicroscopy* **41,** 121–136 (1992).
17. Zou, X. D., Sundberg, M., Larine, M. & Hovmöller, S. *Ultramicroscopy* **62,** 103–121 (1996).
18. Zou, X. D., Sukharev, Y. & Hovmöller, S. *Ultramicroscopy* **52,** 436–444 (1993).

SUPPLEMENTARY INFORMATION. Available on *Nature*'s World-Wide Web Site http://www.nature.com. Paper copies are available from Mary Sheehan at the London editorial office of *Nature*.

ACKNOWLEDGEMENTS. We thank V. Duppel for performing the EDXS analysis. X.D.Z. is supported by an NFR postdoctoral fellowship. S.H. was supported by the Swedish NFR.

CORRESPONDENCE should be addressed to X.D.Z. (e-mail zou@struc.su.se).

Increased activity of northern vegetation inferred from atmospheric CO_2 measurements

C. D. Keeling*, J. F. S. Chin† & T. P. Whorf*

* Scripps Institution of Oceanography, La Jolla, California 92093-0220, USA
† Mauna Loa Observatory, NOAA/CMDL, Hilo, Hawaii 96721, USA

THROUGHOUT **the Northern Hemisphere the concentration of atmospheric carbon dioxide rises in winter and declines in summer, mainly in response to the seasonal growth in land vegetation[1–4]. In the far north the amplitude of the seasonal cycle, peak to trough, is between 15 and 20 parts per million by volume[5]. The annual amplitude diminishes southwards to about 3 p.p.m. near the Equator, owing to the diminishing seasonality of plant activity towards the tropics. In spite of atmospheric mixing processes, enough spatial variability is retained in the seasonal cycle of CO_2 to reveal considerable regional detail in seasonal plant activity[6]. Here we report that the annual amplitude of the seasonal CO_2 cycle has increased by 20%, as measured in Hawaii, and by 40% in the Arctic, since the early 1960s. These increases are accompanied by phase advances of about 7 days during the declining phase of the cycle, suggesting a lengthening of the growing season. In addition, the annual amplitudes show maxima which appear to reflect a sensitivity to global warming episodes that peaked in 1981 and 1990. We propose that the amplitude increases reflect increasing assimilation of CO_2 by land plants in response to climate changes accompanying recent rapid increases in temperature.**

Our most detailed record of the seasonal signal in atmospheric CO_2 has been obtained at Mauna Loa Observatory, Hawaii (20° N, 156° W). We determined the annual amplitude from the interannually detrended record by computing a 4-harmonic seasonal function with invariant phasing, but with linearly increasing amplitude with time, as described in ref. 3. We then estimated this amplitude for each calendar year (Fig. 1*a*, dots in upper plot) by least-square fits of this phase-invariant function to yearly segments of the detrended data. By a second method designed to remove most of the constraint on the computation of amplitude imposed in the first method by a phase-locked signal, we also computed separate 4-harmonic seasonal functions for successive overlapping 3-year segments of the record. The gain of each function was afterwards adjusted to achieve a best fit to the middle year. Annual amplitudes determined by this second method differed only slightly from those determined by the first method. Also, the total gain in amplitude from 1964 to 1994, based on a linear fit to the entire record by the two methods is nearly the same, 20.2 ± 1.4% and 19.7 ± 2.0%, respectively. Here we show amplitudes determined only by the first method. We have observed a similar, although somewhat larger and more irregular, increase in annual amplitude since 1970 at La Jolla, California (33° N, 17° W)[7], confirming that the Mauna Loa record is not exceptional for middle latitudes of the Northern Hemisphere.

The annual amplitude observed at Mauna Loa since 1958 shows almost no trend until the mid-1970s[1]; then it increased almost steadily until 1984; decreased for several years, and increased again to a record maximum in 1991. By smoothing the amplitudes with a spline fit, a quasi-decadal oscillatory pattern is seen with peaks in 1983 and 1992 (solid curve, Fig. 1*a*).

Changes in phase of the Mauna Loa seasonal cycle, characterized by the times of downward zero crossing of the successive harmonic functions, determined by the second method described above, show no trend until the mid-1970s (Fig. 1*a*, lower plot). Thereafter the time of crossing advanced irregularly, becoming about 7 days earlier near the end of the record. Also, the timing of the minimum advanced irregularly after 1980 by about 3 days while the maximum and the upward zero crossing showed no significant long-term changes. These features, taken together, suggest that the growing season of plants has lengthened during approximately the same time period in which the annual amplitude has increased.

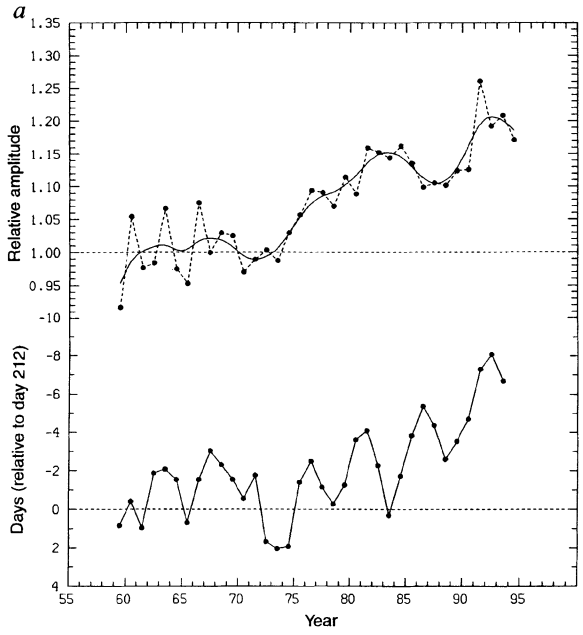

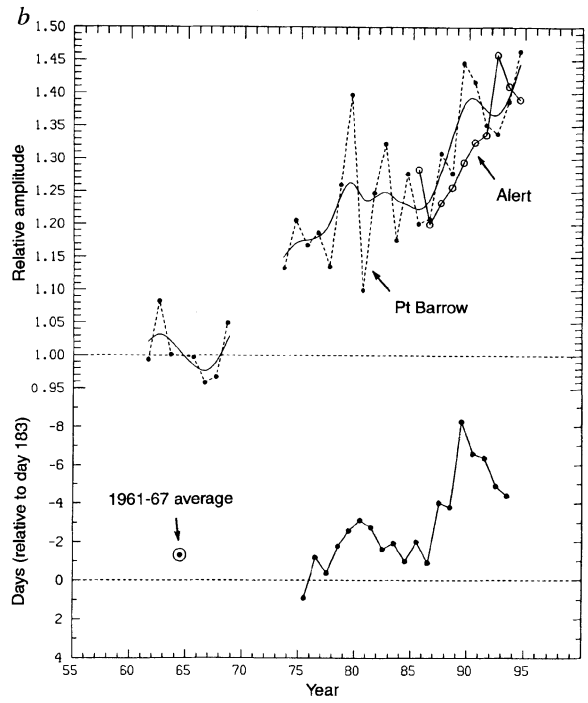

FIG. 1 Trends in relative amplitude and timing of the seasonal cycle of atmospheric CO_2. *a*, At Mauna Loa Observatory, Hawaii. Annual values of the amplitude (upper plot, dots connected by dashed lines) were determined from weekly averaged continuous concentration data[15] fitted annually to a phase-locked 4-harmonic seasonal function. This function, together with a linearly increasing gain factor, was first established by a fit to the full record[3], after which the gain was redetermined separately for each year. The linearly increasing gain factor, referenced to 1964, was computed to be $0.675 \pm 0.045\%$ per year. A smoothing spline[19] (solid curve, with standard error, σ_A, of 0.028%) shows quasi-decadal changes in the relative amplitude. The timing of the downward zero crossing of the seasonal cycle (lower plot, dots connected by solid line segments), was obtained from 3-year fits to the CO_2 record, as described in the text and plotted relative to the 212th day of the year. The zero crossing is with respect to the seasonally adjusted CO_2 concentration determined by the method of ref. 3. *b*, As *a*, but for Point Barrow, Alaska. The data from 1973 to 1994 are from flask samples collected 2–4 times per month, augmented from 1961 to 1967 by continuous CO_2 measurements[8], also calibrated by our laboratory. The fitting procedure (which spans a record gap from 1968 to 1973) yields a linear gain factor of $1.318 \pm 0.100\%$ per year, again referenced to 1964. A smoothing spline (σ_A of 0.050%, as in *a*), shows quasi-decadal changes. Also shown is the trend in amplitude at Alert, Canada (connected open circles in upper plot), plotted so that the sum of the squared annual differences form Point Barrow data, is minimized. The zero crossing time at Point Barrow (lower plot) is plotted relative to the 183rd day of the year. The circled dot in 1964 was determined from 3-year fits for 1961–63 and 1965–67, averaged.

In the Arctic an atmospheric CO_2 record nearly as long as that at Mauna Loa exists for Point Barrow, Alaska (71° N, 157° W)[8,9]. The total gain in annual amplitude from the mean for 1961–67 is 39.5 ± 3.0, approximately twice that at Mauna Loa. The smoothed amplitudes after 1970 show a quasi-decadal pattern not unlike that for Mauna Loa, but with periods of high amplitude near 1980 and 1990 and a low amplitude near 1985 (Fig. 1*b*, upper plot) thus coming sooner than the corresponding periods for Mauna Loa. In addition, large year-to-year fluctuations in amplitude have occurred in the Point Barrow record.

For another Arctic station, at Alert, Canada (82° N, 62° W), with a record beginning in 1985 (open circles in Fig. 1*b*), the annual amplitude generally shows only small year-to-year fluctuations, but has an upward trend similar to that at Point Barrow. The general occurrence of an upward trend in the Arctic and subarctic since 1985 is further confirmed by our harmonic analysis of observations at Mould Bay, Canada and Cold Bay, Alaska[5].

At Point Barrow the time of downward zero crossing (Fig. 1*b*, lower plot) has advanced nearly 7 days since 1975, approximately as at Mauna Loa. The pattern of advance, unlike that at Mauna Loa, tends to be quasi-decadal, approximately in phase with the smoothed amplitude. Other features of the seasonal cycle have varied as well, as at Mauna Loa. Mindful of the gap in the record from 1968 to 1973 we have compared the shape of the average cycle for 1961–67 with that for 1988–94. From the first averaging period to the second, the period of low summertime concentrations has broadened, and the succeeding period of rapidly rising CO_2 comes later in the season than before. In early November when formerly the rate of rise slacked off, in recent years it has continued to rise steeply for another month and a half. These changes, taken together, suggest a progressive lengthening of the growing season, as also suggested by the Mauna Loa record.

We have compared the trend in annual amplitude at Mauna Loa with surface air temperature over land averaged annually between 30° N and 80° N, the zone where most of the seasonal growth of plants takes place in the Northern Hemisphere (see Fig. 3*c* of ref. 6). On the decadal timescale, in which short-term interannual variations are filtered out, the temperature record (upper solid curve of Fig. 2*a*) shows a quasi-decadal pattern with extremes in warmth near 1981 and 1990, about two years before decadal maxima in CO_2 amplitude (lower solid curve). Linear regression of the annual amplitude and temperature data indicate (by lowest χ^2) a lag of between one and two years (see Fig. 2 legend).

We have similarly compared the Point Barrow annual amplitude with land temperatures north of 50° N (Fig. 2*b*), where model simulations[6] indicate that about two-thirds of the Barrow amplitude signal is derived. On the decadal timescale, the temperature record shows a pattern similar to that north of 30° N, with which the CO_2 amplitude is approximately in phase. However, a linear regression of this data gave the lowest χ^2 for amplitude lagging temperature by one year (see Fig. 2).

The observed correlations of annual CO_2 amplitude with land surface temperature suggest large-scale responses of the carbon cycle to climate change. The nature of these responses, however, is not obvious. Neither the signals nor their correlations and lags with temperature were anticipated from prior knowledge of climate or of the global carbon cycle. Some clues as to the possible causes of these signals will now be discussed. We first address long-term increases and then quasi-decadal fluctuations.

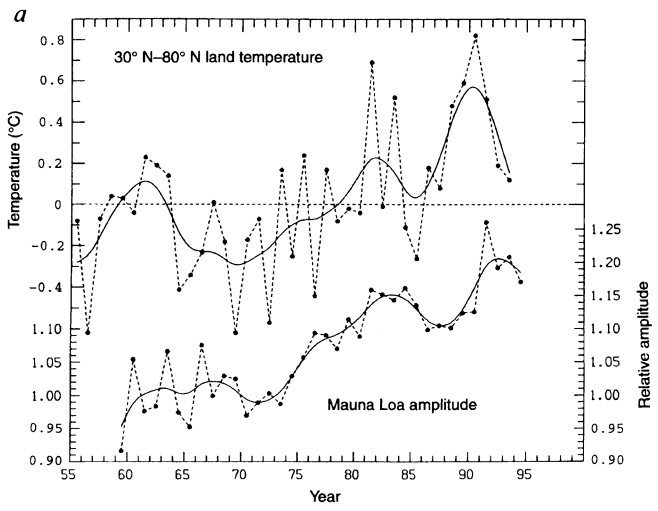

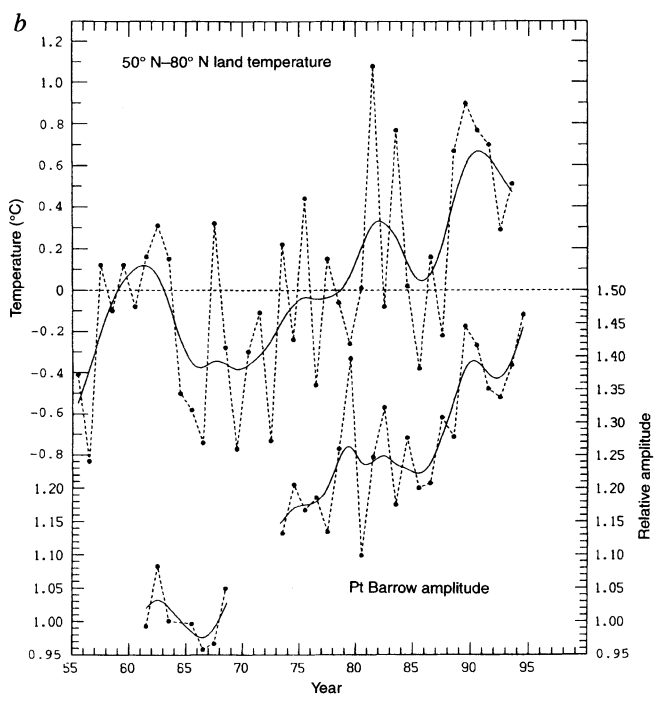

FIG. 2 Comparison of trends in the relative amplitude of the seasonal cycle of atmospheric CO_2 with trends in annual average land temperature. For clarity, the two curves are plotted with visually equivalent scales of linear increase. *a*, Trend in temperature[20] in the zone from 30° N to 80° N (upper plot, annual dots connected by dashed line segments), also shown by a smoothing spline (standard error, σ_T, of 0.215 °C) to reveal quasi-decadal variability. Lower plot, the trend in relative amplitude of CO_2 at Mauna Loa Observatory, as in Fig. 1*a*. The average increase of amplitude with respect to temperature was found by linear regression of annual data, allowing for errors in both variables, represented by σ_A and σ_T, respectively (ref. 21, p. 660). Best-fit estimates based on the lowest χ^2 for the period 1973–94 (for comparison with Point Barrow) showed nearly identical results for lags of one and two years in amplitude relative to temperature, and gave an increase of 19.0 ± 4.0% per °C (reduced $\chi^2 = 1.2$) for the two-year lag. (If run from 1966 to 1994 for a two-year lag, the result was 22.7 ± 3.7% per °C.) *b*, Similar comparison of the amplitude at Point Barrow, Alaska, as in *a*, but using the trend in temperature between 50° N and 80°N (σ_T of smoothing spline 0.320 °C). The best-fit regression in this case was for a lag in amplitude of one year and gave an increase of amplitude with temperature for 1973–94 of 25.5 ± 5.6% per °C (reduced $\chi^2 = 0.9$). Linear correlation coefficients confirmed the lags for both stations.

With respect to long-term changes we focus on the period 1973–94, when we have uninterrupted CO_2 data for both Mauna Loa, Hawaii and Point Barrow, Alaska. Based on linear regressions of annual CO_2 amplitude to temperature over this 21-year period (see Fig. 2 legend), the amplitude at Mauna Loa increased by 19 ± 4% per °C with respect to land temperatures north of 30° N, and Point Barrow by 26 ± 6% per °C with respect to temperature north of 50 °C. Short-term studies indicate that photosynthesis of land plants typically increases by 40–100% for a 10 °C increase in temperature (see p. 147 of ref. 10), with plant respiration (see p. 149 of ref. 10) and soil respiration[11], showing a somewhat larger response. These short-term responses do not approach the high sensitivity to temperature implied by our CO_2 data. Our less-complete data from before 1973 indicate even higher implied sensitivities to temperature.

A few per cent of the overall increase in annual amplitude may be explained by increased seasonality in fossil-fuel combustion and an out-of-phase oceanic cycle, but both effects have been shown by model simulations to be small[6]. Also, the growth of plants is likely to have been stimulated by the 14% increase in ambient CO_2 caused by the rise in global CO_2 concentrations since the beginning of our records, but this effect is predicted[12,13] to explain no more than about a 6% increase in amplitude in 35 years. Changes in atmospheric transport may have contributed to the observed signals, but the general finding of substantial amplitude increases at stations deliberately placed to minimize local influences, makes it unlikely that our conclusions would have been altered by a more-detailed analysis of atmospheric transport.

Thus, the observed annual amplitude increases, especially the large increase found in the Arctic, does not seem to be adequately explained by either direct, short-term responses of plants to temperature or by other factors unrelated to temperature. We propose that an increase in length of the growing season, suggested by changes in timing of the seasonal cycle of CO_2, noted above, may be an important cause of amplitude increases. The finding of Chapman and Walsh[14] that warming at high latitudes has been greatest in winter and spring (up to 4 °C in 30 years) supports this hypothesis.

Any explanation for the recent increases in annual amplitude of CO_2 should also account for its evident correlation with temperature on the decadal timescale. In this connection we note that the abundance of atmospheric CO_2, also appears to correlate decadally with temperature[15], as though variations in the seasonal cycle of CO_2 have caused imbalances in the annual exchange of plant CO_2 with the atmosphere. We now discuss this possibility.

Interannual variations in atmospheric CO_2 abundance are partly contributed by oceanic processes, but model simulations suggest that the quasi-decadal signal in abundance has been predominantly terrestrial[9], and therefore should largely reflect imbalances between the uptake of CO_2 by vegetation, expressed as net primary production (NPP), and release of CO_2 from plant litter and soils, caused by heterotrophic respiration (HR). Because the seasonal signal in CO_2 is caused mainly by NPP during summer and by HR during winter, (though always made up of NPP – HR), the phase relationship between the decadal signals in amplitude and in abundance should be related to how interannual variations in NPP and HR have affected both signals.

Over the time period of atmospheric CO_2 measurements, quasi-decadal variations in CO_2 abundance have been observed to be nearly in phase with quasi-decadal variations in global temperature[9,15] which have nearly the same phasing as the temperatures north of 30° N, shown in Fig. 2. The decadal signal in the annual average net ecosystem flux, NPP – HR, has therefore lagged temperature by a quarter of a cycle, that is, by approximately two years. Because the observed quasi-decadal signal in annual CO_2 amplitude, as shown in Fig. 2*a*, has also lagged temperature by about two years, decadal maxima in amplitudes have evidently occurred approximately when annual NPP has maximally exceeded annual HR, and *vice versa*.

These phase relations suggest that NPP, on a decadal timescale

has been stimulated when it warms and diminished when it cools, with the response lagging temperature. Heterotrophic respiration, HR, may have also been affected, either directly or in response to the changes in NPP, in a manner to produce a two-year phase lag in the difference, NPP – HR. Variations in mean annual temperature have been too small to be a likely direct cause of such variations, but coherent variations in the length of the growing season, especially at higher latitudes, may well have produced large variations in NPP with consequent variations in HR.

Although the quasi-cyclic variations in the carbon cycle seen in our data would therefore appear to arise from natural variability in temperature, this variability is not obviously the cause of the longer-term increases in annual CO_2 amplitude reported here. These striking increases over 30 years could represent unprecedented changes in the terrestrial biosphere, partially in response to some of the highest global annual average temperatures since the beginning of modern records[16,17], and partially in response to plant growth being stimulated by the highest concentrations of atmospheric CO_2 in the past 150,000 years (ref. 18). □

Received 19 April; accepted 20 May 1996.

1. Hall, C. A. S., Ekdahl, C. A. & Wartenberg, D. E. *Nature* **255,** 136–138 (1975).
2. Pearman, G. I. & Hyson, P. *J. geophys. Res.* **85,** 4468–4474 (1980).
3. Bacastow, R. B., Keeling, C. D. & Whorf, T. P. *J. geophys. Res.* **90,** 10529–10540 (1985).
4. D'arrigo, R., Jacoby, G. C. & Fung, I. Y. *Nature* **329,** 321–323 (1987).
5. Conway, T. J. *et al. J. geophys. Res.* **99,** 22831–22855 (1994).
6. Heimann, M., Keeling, C. D. & Tucker, C. J. in *Aspects of Climate Variability in the Pacific and the Western Americas* (ed. Peterson, D. H.) 277–303 (Am. Geophys. Union, Washington DC, 1989).
7. Whorf, T. P. & Keeling, C. D. *Summary Report 1990*, 124–126 (Climate Modeling & Diag. Lab. Vol. 19, NOAA, Boulder, CO, 1991).
8. Kelley, J. J. Jr *Scientific Report, Contract N00014-67-A-0103- 0007 NR 307-252* (US Office of Naval Research, Arctic Program, Washington DC, 1969).
9. Keeling, C. D. *et al.* in *Aspects of Climate Variability in the Pacific and the Western Americas* (ed. Peterson, D. H.) 165–236 (Am. Geophys. Union, Washington DC, 1989).
10. Larcher, W. *Ökologie der Pflanzen* (Ulmer, Stuttgart, 1984).
11. Raich, J. W. & Schlesinger, W. H. *Tellus* **44B,** 81–99 (1992).
12. Kohlmaier, G. H. *et al. Tellus* **41B,** 487–510 (1989).
13. Luo, Y. & Mooney, H. A. in *Responses of Terrestrial Ecosystems to Elevated* CO_2 (eds Koch, G. W. & Mooney, H. A.) 381–397 (Academic, San Diego, in the press).
14. Chapman, W. L. & Walsh, J. E. *Bull. Am. met. Soc.* **74,** 33–47 (1993).
15. Keeling, C. D., Whorf, T. P., Wahlen, M. & van der Plicht, J. *Nature* **375,** 666–670 (1995).
16. Aldhous, P. *Nature* **349,** 186 (1991).
17. Jones, P. D. & Briffa, K. R. *Global Surface Air Temperature Variations during the Twentieth Century* Part 1, *Spatial, Temporal and Seasonal Details, Holocene 2.2*, 165–179 (Climate Res. Unit, Univ. East Anglia, Norwich, 1992).
18. Barnola, J. M., Raynaud, D., Korotkevich, Y. S. & Lorius, C. *Nature* **329,** 408–414 (1987).
19. Reinsch, C. H. *Numerische Mathematik* **10,** 177–183 (1967).
20. Jones, P. D. *J. Clim.* **7,** 1794–1802 (1994).
21. Press, W. H., Tevkolsky, S. A., Vetterling, W. T. & Flannery, B. P. *Numerical Recipes in Fortran* 2nd edn (Cambridge Univ. Press, 1992).

ACKNOWLEDGEMENTS. We thank P. Jones for providing monthly gridded surface air temperature data; P. Tans, N. Trivett and their associates for assistance over many years in acquiring atmospheric data at Mauna Loa Observatory, Point Barrow, Alaska, and Alert Station, Canada; and R. Bacastow, R. Hunt, R. Keeling, J. Kelley, S. Piper and J. Walsh for their advice. This work was supported by the US NSF, the US Department of Energy, NASA and NOAA.

CORRESPONDENCE should be addressed to C.D.K. (e-mail cdkeeling@ucsd.edu).

Structural control on sea-floor hydrothermal activity at the TAG active mound

Martin C. Kleinrock* & Susan E. Humphris†

* Department of Geology, Vanderbilt University, Nashville, Tennessee 37235, USA
† Department of Geology and Geophysics, Woods Hole Oceanographic Institution, Woods Hole, Massachusetts 02543, USA

THE TAG active mound[1–13], on the Mid-Atlantic Ridge near 26° N, is one of the largest known, actively forming volcanogenic massive sulphide deposits. Construction of such a deposit requires that the upflow of hydrothermal fluids be localized at this site over tens of thousands of years, but the cause of this localization has been controversial. Two popular hypotheses propose that it results from young volcanism immediately adjacent to the mound[6], or from the intersection of a 'transfer fault', orthogonally crossing the rift-valley floor, with ridge-parallel faults[8]. Here we present high-resolution sonar and photographic data which provide no evidence for young eruptions nearby, or for transverse, through-going faults intersecting the TAG mound. Instead, our data suggest that the localization of hydrothermal activity at the TAG mound is strongly controlled by permeable conduits at the intersection of an actively developing ridge-parallel fissure/fault complex with a newly recognized but older, oblique fault system. These observations may aid the interpretation of similar structures in ancient sea-floor sulphide deposits, where the tectonic disruption caused by emplacement on land has obscured the original geometry.

Today, hydrothermal activity at temperatures above 25 °C in the TAG (Trans-Atlantic Geotraverse) area is confined to the ~200-m-diameter active mound, 26° 8.2′ N, 44° 49.5′ W (Fig. 1). This mound of polymetallic sulphides and massive anhydrite[11], located near the Mid-Atlantic Ridge median valley wall ~3 km east of the neovolcanic axis, appears to have been active episodically for at least 20,000 years (refs 7 and 12), and is estimated to contain about 3.9 million tonnes of sulphides[13]. We collected high-resolution sidescan sonar imagery with co-registered bathymetry of a 10 × 10 km region of the rift valley and detailed photography (including over 30,000 electronic still camera images) from the mound and its environs using the deeply towed ARGO-II and DSL-120 instrument packages[14–16].

Based primarily on the 120-kHz sidescan data, we divide the rift valley in this area into four distinct morphological zones (Fig. 2): a neovolcanic zone, an active fissure/fault zone, and eastern and western terraced zones. The TAG active hydrothermal mound (Figs 2 and 3) lies within the active fissure/fault zone at the intersection of rift-parallel N-to-NNE-striking faults and fissures and a set of newly identified, older ENE-striking faults. Within ~50 m to the east of the mound, we observed a 20-m-high westward-dipping fault striking NNE (Fig. 3*a*). The presence of fresh talus at the base of this fault and other NNE faults within this zone, combined with a progressive eastward increase in fissure/fault length and throw[17], show that this area is actively extending and the rift-parallel NNE structures are still developing.

Bathymetric and sonar images constructed from our new data (Fig. 3) present the first synoptic view of the shape and nature of the TAG active mound. The distinctly circular, 200-m-diameter mound shoals to a depth of 3,630 m, ~50 m above the surrounding sea floor. The mound comprises two well defined platforms, a lower 150-m-diameter platform at 3,650–3,655 m and an upper 90-m-diameter platform at 3,642–3,650 m. The upper platform contains the previously described[4,10,11] primary black-smoker complex and a NNE-trending depression that was absent during previous studies in 1986–90. The alignment of this depression with NNE-trending faults and fissures just north and south of the mound suggest that the mound is being extended WNW–ESE in concert with its environment. Whereas previous studies found black-smoker venting only at the primary black-smoker complex[11], we observe a new and separate suite of black-smoker vents on the upper platform, many along fissures near or within this depression (Fig. 4). These changes suggest recent surficial collapse linked to continuing fissure/fault development, perhaps with associated changes in the subsurface permeability and fluid pathways. The generation of the new depression atop the mound and the coincident development of new black-smoker vents show that contemporaneous tectonic deformation and hydrothermal deposition modified the three-dimensional structure and hydrogeology of the TAG active mound shortly before our survey.